Hydrology Research

Hydrology Research Vol 52 No 4, 847 doi: 10.2166/nh.2021.135

Annual nitrate load patterns in an agricultural watershed in consecutive dry years

Shuai Chen [a,b] and Xiaohong Ruan [a,b,*]
[a] Key Laboratory for Surficial Geochemistry of the Ministry of Education, Nanjing University, Nanjing 210023, China
[b] School of Earth Sciences and Engineering, Nanjing University, Nanjing 210023, China
*Corresponding author. E-mail: ruanxh@nju.edu.cn

SC, 0000-0003-1629-7278

ABSTRACT

Nitrate (NO_3-N) load characteristics in consecutive dry years in the Huai River Basin (HRB), China, were examined using streamflow and NO_3-N concentration data. The data set spanned 12 years including three consecutive dry years. Baseflow separation, load estimation, and nonparametric linear regression were applied to separate point source (PS), baseflow, and surface runoff NO_3-N loads from the total load. The mean annual nonpoint source (NPS) load was 2.84 $kg{\cdot}ha^{-1}{\cdot}yr^{-1}$, accounting for 90.8% of the total load. Baseflow contributed approximately one-fourth of the natural runoff and half of the NPS load. The baseflow nitrate index (i.e., the ratio of baseflow NO_3-N load to total NPS NO_3-N load) was 25.4% higher in consecutive dry years than in individual dry years. This study demonstrated that baseflow is the preferential hydrological pathway for NO_3-N transport in the HRB and that baseflow delivers a higher NO_3-N percentage to streams under long-term drought than under short-term drought. This study highlights the alarming evidence that continuous drought caused by climate change may lead to a higher rate of nitrogen loss in agricultural watersheds.

Key words: agricultural watershed, baseflow, baseflow enrichment ratio, consecutive dry years, Huai River Basin, nitrate load

HIGHLIGHTS

- Baseflow is the preferential hydrological pathway for nitrate transport in the Huai River Basin.
- Baseflow delivers a higher percentage of nitrate to streams in consecutive dry years than in individual dry years.
- The combination of baseflow separation, load estimation, and nonparametric linear regression provides a convenient method to differentiate the nitrate load from different sources.

INTRODUCTION

The Huai River Basin (HRB), where the annual nitrogen fertilizer application rates amount to approximately 600 $kg{\cdot}N{\cdot}ha^{-1}{\cdot}yr^{-1}$, is one of the major grain-producing areas in China. Nitrogen fertilizers have been identified as the main contributor to the increases in the nitrate-nitrogen (NO_3-N) concentration in groundwater in agricultural watersheds (Czekaj *et al.* 2016; Coskun *et al.* 2017; Paladino *et al.* 2020; Wu *et al.* 2021), and the HRB is no exception (Ju & Zhang 2017). The NO_3-N concentration in groundwater below agricultural fields is generally much higher than in surface waters (Almasri & Kaluarachchi 2004). This NO_3-N in groundwater may be primarily transferred to surface waters under baseflow conditions (He & Lu 2016; Richards *et al.* 2021). However, apart from Chen (2013) and Chen *et al.* (2017), who estimated the NO_3-N load in groundwater discharge in a small sub-basin, few researchers have reported the long-term baseflow contributions to the nonpoint source (NPS) NO_3-N loads in streamflows in the HRB. Therefore, it is necessary to quantify the NPS NO_3-N loads and baseflow contribution for NPS NO_3-N assessment and management of the HRB.

Climate change is likely to make hydrological regimes more extreme, with wet seasons becoming wetter and dry seasons becoming drier. The runoff from the upper and middle HRB has decreased over the last 60 years because of regional climate change and human activities, implying that the risks and intensity of droughts have increased (An & Hao 2017). Consecutive dry years, such as those occurring from 2011 to 2013, will probably occur more frequently in the future. These changes may influence the temporal variations in NPS NO_3-N loads. Many researchers have reported that the NO_3-N loads transported from agricultural watersheds to surface waters are low in low-flow periods, owing to the reduced runoff, but will increase

after droughts end (Schilling & Zhang 2004). However, few studies focus on the impact of long-term droughts persisting over many years on baseflow NO_3-N loads. If carrying much NO_3-N, baseflow as the main source of environmental flow in dry periods (de Graaf *et al.* 2019) may threaten the health of riverine ecosystems under long-term drought. Within the context of climate change, to support the development of effective policies to manage the water quality, such as total maximum daily load programs and best management practices, the impact of consecutive dry years on baseflow NO_3-N loads needs to be evaluated.

Traditionally, constituent loads are calculated as the product of the discharge volume and constituent concentration in water. However, no direct approach exists at present to continuously measure baseflow and the constituent concentration in baseflow. One of the common methods is to estimate the baseflow NO_3-N load by assuming the streamflow NO_3-N concentration, with a baseflow index (BFI, i.e., the ratio of baseflow to total streamflow) $\geq$90 or 80% as the real baseflow concentration combined with baseflow separating methods and load estimation programs (e.g., LOADEST; Runkel *et al.* 2004; He & Lu 2016). However, this method may be problematic when applied to regions where the point source (PS) NO_3-N load cannot be neglected, because the assumed baseflow NO_3-N concentration (i.e., streamflow NO_3-N concentration at BFI $\geq$90 or 80%) consists of both PS and baseflow contributions. Therefore, the PS NO_3-N load needs to be quantified when applying this method to estimate the baseflow NO_3-N load. However, it is difficult to directly quantify the PS contributions for regions like the HRB, where the NO_3-N concentration is not a routine monitoring item of sewage outfalls, in addition to the influence of the chemical and biological transformations between the source and monitoring station (Albek 2003). Albek (2003) provided an indirect method – the Kendall–Theil robust line (KTRL) regression method (Helsel & Hirsch 1992) – to estimate the PS constituent load based on discharge and concentration data measured at monitoring stations. This approach assumes that the PS constituent load remains constant over a given period and is estimated as the slope of the KTRL. In this study, the NO_3-N loads consisting of PS, baseflow, and surface runoff contributions at the outlet of the upper and middle HRB were estimated via a combination of baseflow separation, load estimation, and KTRL regression, as described above.

The main objectives of this study are to (1) quantify the total NPS NO_3-N loads exported from the upper and middle HRB and quantify the baseflow contribution, (2) identify the preferential hydrological pathway of NO_3-N transport, and (3) evaluate the impact of consecutive dry years on the baseflow NO_3-N loads.

STUDY AREA AND DATA

Watershed description

The study site is the watershed above the Bengbu Hydrometric Station (Figure 1). The area of the watershed is 121,330 km^2. The study area mainly comprises hills and flatlands, which account for 71% of the watershed area. The quaternary layers have a thickness ranging from 50 to 200 m and mainly consist of fluvial and lacustrine loose sediments. The main aquifer is the quaternary unconsolidated rock, which is separated into shallow and deep aquifers by a thick layer of clayey soil. The thickness of shallow aquifer ranges from 50 to 60 m and the buried depth of shallow groundwater ranges from 2 to 6 m (Ge *et al.* 2006). The mean annual precipitation is 911 mm. The flood season lasts from June to September, and the dry season lasts from December to February. Rainfall accounts for 60% of the annual precipitation in the flood season (Figure 1(d)).

In general, most of the rivers are recharged by groundwater all year round (Pan 2014). Figure 2 shows the monthly river stages measured at four gauging stations (Figure 1(c)) from 2011 to 2012 and the nearby groundwater levels. It is evident that the groundwater levels are higher than surface water levels.

The agriculture, urban, and forest land account for 70.1, 14.2, and 6.8% of the watershed area, respectively. As a major grain-producing area in China, the study area is dominated by dry land crops and the application rate of chemical fertilizer (600 $kg{\cdot}ha^{-1}{\cdot}yr^{-1}$) ranks first in the country (Ju & Zhang 2017). Agricultural food processing, leather manufacturing, and papermaking are the main industries in this area.

Data

This study is based on daily stream discharge data collected from 2007 to 2018 at the Bengbu Station, which is operated by the Huai River Commission of the Water Resources Ministry of the P.R.C. The baseflow was extracted from the streamflow using the digital filter method. The wastewater discharge data originated from the Huai River Water Resources Bulletin (http://www.hrc.gov.cn). The precipitation data were downloaded from the National Meteorological Information Center (http://data.cma.cn/site).

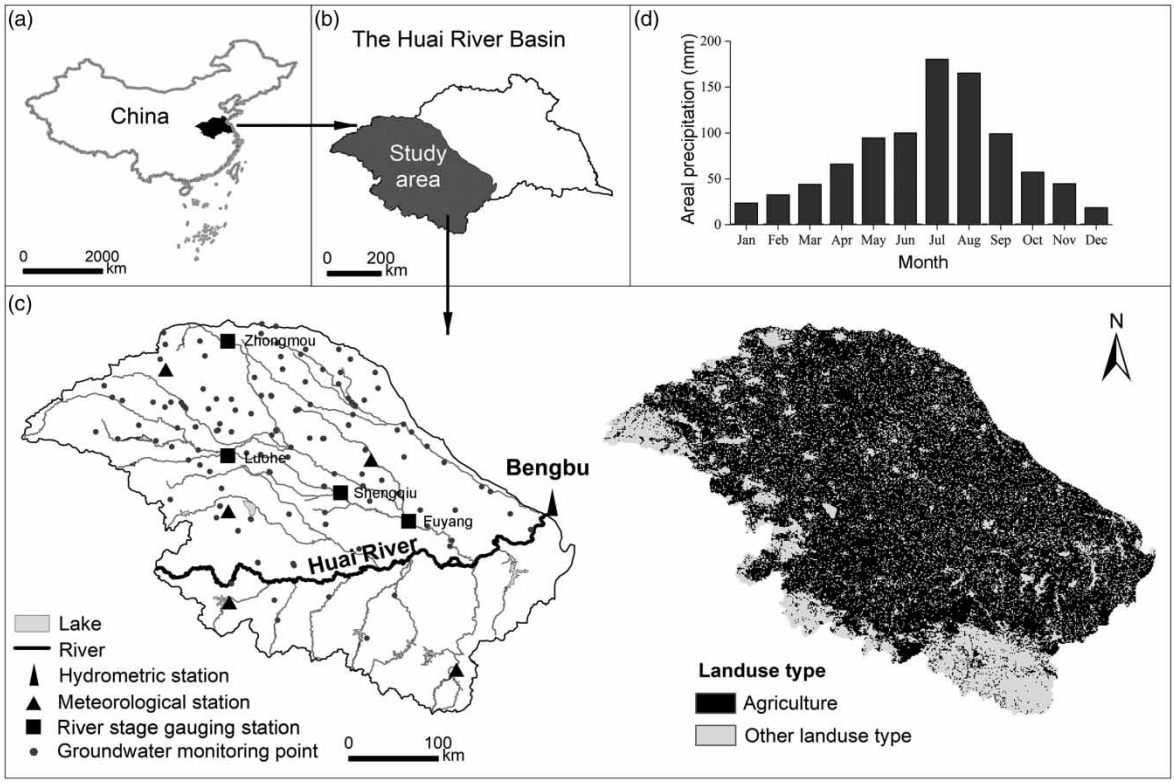

Figure 1 | (a,b) Location of the study area, (c) sampling sites and land use types, and (d) seasonal variations in the areal precipitation.

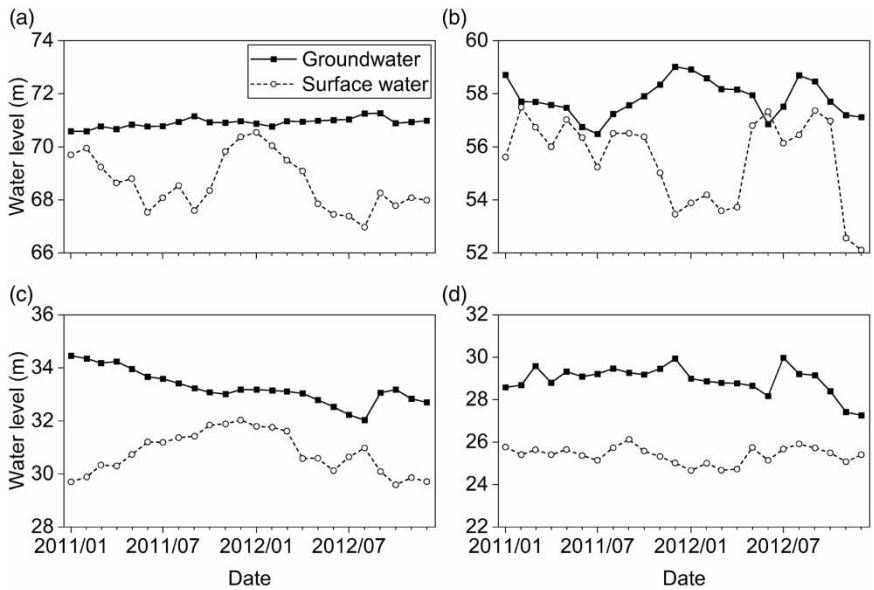

Figure 2 | Monthly river stages measured at (a) Zhongmou, (b) Luohe, (c) Shengqiu, and (d) Fuyang gauging stations from 2011 to 2012 and the nearby groundwater levels.

A total of 128 surface water samples were collected at the Bengbu Station from 2007 to 2018, either monthly or bimonthly. Groundwater quality samples were collected from 122 phreatic wells (Figure 1(c)) in both the flood and non-flood seasons between 2007 and 2018, excluding 2013. The NO_3-N concentrations were determined in the laboratory by ultraviolet

spectrophotometry (detection limit = 0.08 mg/L). The NO_3-N concentration in the surface water samples ranged from 0.31 to 4.45 mg/L, with an average of 2.05 mg/L (Figure 3(a)). It was generally the highest when the streamflow was low. The result of a seasonal Kendall test (Helsel & Hirsch 1992) suggests that from 2007 to 2018, the streamflow NO_3-N concentration exhibited no significant temporal trend ($p > 0.05$), indicating that the entire data set could be grouped together for analysis purposes. The streamflow NO_3-N concentration on days when BFI $\geq$ 90% was assumed to be caused by the PS and baseflow NO_3-N loads. This NO_3-N concentration ranged from 1.52 to 4.45 mg/L with an average of 2.86 mg/L. The annual average groundwater NO_3-N concentration over the 122 monitoring wells (Figure 1(c)) ranged from 4.12 mg/L in 2017 to 9.34 mg/L in 2008 (Figure 3(b)). The maximum groundwater NO_3-N concentration reached 75.9 mg/L. This was much higher than the surface water NO_3-N concentration.

METHODOLOGY

Overall procedures

In this study, the total streamflow was assumed to be composed of discharge from sewage outfalls, baseflow, and surface runoff. The discharge from sewage outfalls was termed as anthropogenic PS discharge, and the total discharge subtracted by the anthropogenic PS discharge was termed as natural discharge (i.e., baseflow plus surface runoff). Anthropogenic PS discharge can obscure the contributions from surface runoff and baseflow to a streamflow hydrograph when using digital filter methods (Barlow *et al.* 2015). Therefore, the anthropogenic PS discharge was removed from the total flow before baseflow separation. Baseflow was separated from the natural streamflow using the recursive digital filter method proposed by Eckhardt (2005). The total NO_3-N load consisted of PS and NPS contributions (i.e., anthropogenic PS discharge and the natural streamflow, respectively). First, the total load and the PS and baseflow loads were estimated using regression estimator LOADEST (Runkel *et al.* 2004). This regression estimator assumes that the relationship between the logarithms of the constituent concentration and discharge is approximately linear (Cohn *et al.* 1989). Second, the PS load was estimated using the method proposed by Albek (2003) with confining conditions. Finally, the surface runoff load and baseflow load were extracted from the total load and the PS and baseflow loads, respectively. For the purpose of comparison, the annual discharges were converted into millimeters, and the annual loads were calculated as the average daily load multiplied by the number of days per year and divided by the drainage area, including the PS discharge and PS load.

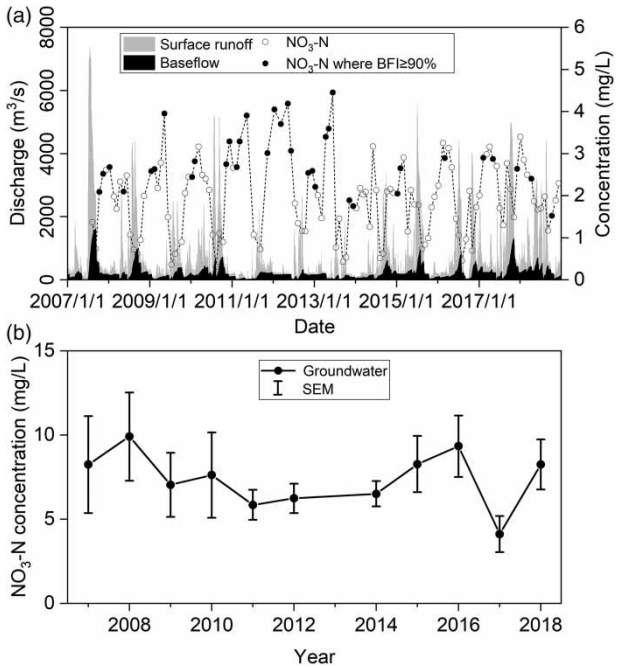

Figure 3 | (a) Time series of the daily baseflow and surface runoff and streamflow NO_3-N concentrations observed at the Bengbu Station from 2007 to 2018 and (b) annual variations in the spatially averaged (over all the groundwater monitoring sites) groundwater NO_3-N concentration. SEM, standard error of mean.

Baseflow separation

The natural flow was extracted from the total flow before baseflow separation:

$$Q_{n,k} = Q_{t,k} - Q_p \tag{1}$$

where Q_n is the natural streamflow, k is the time step, Q_t is the total streamflow, and Q_p is the PS discharge, which remains constant over a given period. Assuming that the outflow from an aquifer is linear to its storage (Eckhardt 2008), the recursive digital filter method divides the natural flow into surface runoff and baseflow. The filter is expressed as follows:

$$Q_{b,k} = \frac{(1 - \mathrm{BFI}_{max})\alpha Q_{b,k-1} + (1-\alpha)\mathrm{BFI}_{max} Q_{n,k}}{1 - \alpha \mathrm{BFI}_{max}} \tag{2}$$

$$Q_{s,k} = Q_{n,k} - Q_{b,k} \tag{3}$$

The filter is subject to $Q_{b,k} \leq Q_{n,k}$, where Q_b is the baseflow, Q_s is the surface runoff, BFI_{max} and α are filter parameters. The filter parameter BFI_{max} was set to 0.8 in this study, which, according to Eckhardt (2005), is suitable for perennial streams and porous aquifers. Filter parameter α was set to 0.9982, which was determined by recession analysis according to Eckhardt (2008).

NO_3-N load estimation

Two user-defined regression models were built in LOADEST to estimate the total NO_3-N load (Model 1) and the PS and baseflow NO_3-N loads (Model 2), as described in the following equations, respectively (Runkel *et al.* 2004):

$$L_t = \exp(a_0 + a_1 \ln(\widetilde{Q_t}) + a_2 \ln(\widetilde{\mathrm{BFI}}) + a_3 \ln(\widetilde{P_L}) + a_4 \sin(2\pi\widetilde{d_{time}}) + a_5 \cos(2\pi\widetilde{d_{time}}) + a_6 \widetilde{d_{time}})g_t \tag{4}$$

$$L_{pb} = \exp(b_0 + b_1 \ln(\widetilde{Q_p + Q_b}) + b_2 \ln(\widetilde{P_L}) + b_3 \sin(2\pi\widetilde{d_{time}}) + b_4 \cos(2\pi\widetilde{d_{time}}) + b_5 \widetilde{d_{time}})g_{pb} \tag{5}$$

where a_j and b_j are model coefficients, L_t is the estimated total NO_3-N load, L_{pb} is the estimated NO_3-N load consisting of PS and baseflow contributions. g_t and g_{pb} are bias correction factors. $\ln(\widetilde{Q_t})$, $\ln(\widetilde{\mathrm{BFI}})$, $\ln(\widetilde{P_L})$, and $\ln(\widetilde{Q_p + Q_b})$ are the centered values of the natural logarithms of the total streamflow, *BFI*, annual precipitation in the last year, and summation of the PS discharge and baseflow, respectively. $\widetilde{d_{time}}$ is the centered decimal time. The explanatory variables are centered to eliminate collinearity, and the center of a variable can be found in Runkel *et al.* (2004).

The explanatory variables in Model 1 (Equation (4)) are chosen to consider the influence of the total streamflow, BFI, antecedent precipitation, and seasonal factors, such as agricultural activities and temperature, which are major drivers of biological, chemical, and physical processes. Model 2 (Equation (5)) considers the influence of baseflow, antecedent precipitation, and seasonal factors. The model coefficients (a_j and b_j) in Equations (4) and (5) were calculated using the maximum likelihood estimator (MLE) (Cohn *et al.* 1989). The MLE assumes that the model residuals follow a normal distribution with a constant variance. The calibration period ranged from 2007 to 2018. The coefficients in Model 1 were calibrated by the streamflow NO_3-N concentration ($n = 128$). The coefficients in Model 2 were calibrated by the streamflow NO_3-N concentration on days when the BFI was between 90 and 100% ($n = 35$).

The PS NO_3-N load was estimated based on the mass balance (Albek 2003):

$$C_t Q_t = C_p Q_p + C_n Q_n \tag{6}$$

where C_t, C_p, and C_n are the NO_3-N concentrations in the total streamflow, PS discharge, and natural runoff, respectively. If the total streamflow is much greater than the PS discharge (i.e., $Q_t \gg Q_p$), Q_n can be replaced by Q_t and Equation (6) can be written as follows:

$$C_t = L_{p,\mathrm{KTRL}}/Q_t + C_n \tag{7}$$

where $L_{p,\mathrm{KTRL}} = C_p Q_p$, which is the initially estimated PS NO_3-N load and is constant over a given period. This can be estimated by linear regression of C_t against $1/Q_t$. For nonparametric linear regression, the KTR has been recommended to

eliminate the effects of data outliers and to avoid any restrictions posed by normality assumptions (Helsel & Hirsch 1992). In this study, $L_{p,\,KTRL}$ was estimated in three time periods (2007–2010, 2011–2013, and 2014–2018) to account for the annual variations in the PS NO_3-N load.

Assuming that the PS NO_3-N load will remain constant over a given period and should be no higher than the NO_3-N loads consisting of PS and baseflow contributions (L_{pb}), the upper limit of the PS NO_3-N load for a given year can be written as follows:

$$L_{p,\,u}(i) = \min\{L_{pb}i, j | 1 \le j \le 365 \text{ or } 366\} \quad i = 2007,\ 2008,\ \ldots,\ 2018 \tag{8}$$

where $L_{p,\,u}$ is the upper limit of the PS NO_3-N load, i is the year, and j is the jth day of year i. Finally, the PS NO_3-N load in this study is estimated as follows:

$$L_p(i) = \min\{L_{p,\,KTRL}(i),\ L_{p,\,u}i\} \quad i = 2007,\ 2008,\ \ldots,\ 2018 \tag{9}$$

where L_p is the final result of the PS NO_3-N load estimation.

The surface runoff, baseflow, and total NPS NO_3-N loads are estimated as follows:

$$L_s = L_t - L_{pb} \tag{10}$$

$$L_b = L_{pb} - L_p \tag{11}$$

$$L_n = L_s + L_b = L_t - L_p \tag{12}$$

where L_s, L_b, and L_n are the estimated surface runoff, baseflow, and total NPS NO_3-N loads, respectively. The baseflow nitrate index (BFNI, i.e., the ratio of baseflow NO_3-N load to total NPS NO3-N load) is calculated as follows:

$$\text{BFNI} = \frac{L_b}{L_n} \times 100\% \tag{13}$$

where BFNI represents the baseflow contribution to the total NPS NO_3-N load. The baseflow enrichment ratio (BER) is used to describe the preferential pathway of NO_3-N transport (Schilling & Zhang 2004). The BER is calculated as follows:

$$\text{BER} = \text{BFNI}/\text{BFI} \tag{14}$$

If NO_3-N essentially followed the water flow, then the BFNI would be equal to the BFI and the BER would equal 1. A BER value greater than 1 implies that NO_3-N is preferentially leached into groundwater and carried by the baseflow to streams.

RESULTS

Parameters calibration

The coefficients for Model 1 (Equation (4)) and Model 2 (Equation (5)) are presented in Table 1. The scatter plots of the observed load versus the estimated load are shown in Figure 4(a) and 4(b), and the correlation coefficients for Models 1 and 2 were all larger than 0.83. The scatter plots and normal probability plots for the model residuals (Figure 4(c)–4(f)) indicate that the residuals of the two models adhere to the normal distribution and constant variance assumptions of the MLE. The significance level ($p > 0.05$) of the independent-sample t-test for the model residuals in the consecutive dry years (2011–2013) versus the other years indicates that climate conditions exhibited no significant differences between the consecutive dry years and the other years to the models. Therefore, it is appropriate to fit only one model for the entire study period when estimating the total NO_3-N load or the PS and baseflow NO_3-N loads. The bias percentage (Bp), Nash–Sutcliffe efficiency (NSE), and ratio of the root mean square error to the standard deviation of the measured data (RSR) were −2.53, 0.773, and 0.428 for Model 1, respectively, and 0.629, 0.755, and 0.443 for Model 2, respectively. The accuracy of the model simulations obtained in this study was satisfactory according to Moriasi *et al.* (2007), who recommended that model simulations could be considered satisfactory when NSE >0.50 and RSR ≤0.70.

Table 1 | Model coefficients, regression statistics, and bias diagnostics for Models 1 and 2

Items	Model 1	Model 2
Model coefficients	$a_0 = 9.651$; $a_1 = 0.908$; $a_2 = 0.006$; $a_3 = 0.243$; $a_4 = -0.256$; $a_5 = 0.409$; $a_6 = 0.017$	$b_0 = 13.453$; $b_1 = 0.995$; $b_2 = -0.434$; $b_3 = 0.055$; $b_4 = -0.014$; $b_5 = 0.191$
Regression statistics		
R^2	0.834	0.839
S^2	0.166	0.049
PPCC	0.991	0.993
p^a	0.967	0.907
p^b	0.421	0.126
Bias diagnostics		
Bp	−2.53	0.629
NSE	0.773	0.755
RSR	0.428	0.443

[a]The PPCC test is at a significance level of 0.05.
[b]The independent-sample *t*-test for the model residuals in the consecutive dry years versus the other years at a significance level of 0.05.
R^2, coefficient of determination; S^2, residual variance; PPCC, probability plot correlation coefficient; Bp, bias percentage; NSE, Nash–Sutcliffe efficiency index; RSR, ratio of the root mean square error to the standard deviation of the measured data.

Baseflow

The mean annual precipitation and runoff in the upper and middle reaches of the HRB were 932.7 and 237.2 mm, respectively, during our study period. The annual runoff series (1956–2018) were analyzed via frequency analysis based on the Pearson Type III distribution to identify the annual hydrological patterns in the study area. The results indicate that the period from 2011 to 2013 was continuously dry, 2009 was also dry, 2007 and 2017 were wet, and the other years were normal.

From 2007 to 2018, the annual PS discharge increased from 14.6 to 22.5 mm (Table 2). The mean annual PS discharge was 17.5 mm, accounting for 9.0% of the total discharge (194.6 mm). The mean annual baseflow and surface runoff were 47.1 and 130.0 mm, accounting for 19.5 and 71.5% of the total discharge, respectively. Because of the reduced precipitation, the baseflow and surface runoff were lower in the consecutive dry years (2011–2013) than in the individual dry year (2009) and the other normal or wet years (Figure 5(a)). The coefficient of variance (CV) of the daily baseflow and surface runoff was 1.25 and 1.80, respectively. This result suggests that the baseflow was less variant than the surface runoff. Over the study period, the annual BFI ranged from 20.3 to 34.6% with an average of 26.6%. The BFI was the highest in the consecutive dry years, with an average of 33.0%, which was higher than the BFI in the individual dry year (24.6%) and the mean annual BFI (Figure 5(c)). In general, the BFI tended to increase in drier years because less precipitation was routed to streams as surface runoff, while the baseflow remained relatively steady.

PS NO_3-N load

The PS NO_3-N loads estimated by KTRL regression ($L_{p,\ KTRL}$) were 23.6, 10.5, and 4.1 t/d for the time periods of 2007–2010, 2011–2013, and 2014–2018, respectively (Figure 6). The upper limit of the PS NO_3-N load is shown in Figure 7. It decreased from 17.5 t/d in 2007 to 11.1 t/d in 2018. The final PS load (L_p), estimated from Equation (9), ranged from 17.5 t/d (0.53 $kg{\cdot}ha^{-1}{\cdot}yr^{-1}$) to 4.1 t/d (0.12 $kg{\cdot}ha^{-1}{\cdot}yr^{-1}$), which also exhibited a decreasing trend (Table 2; Figure 5(b)). It decreased by 77% from 2007 to 2018. The mean annual PS load was 9.7 t/d (0.29 $kg{\cdot}ha^{-1}{\cdot}yr^{-1}$), which accounted for 9.2% of the total load, and the mean annual PS load in the consecutive dry years was 10.6 t/d (0.32 $kg{\cdot}ha^{-1}{\cdot}yr^{-1}$), which accounted for 22.2% of the total load. Because of the reduced natural runoff in the consecutive dry years, the NPS load decreased, but the proportion of the PS load increased.

NPS NO_3-N load

The total NPS NO_3-N loads ranged from 1.03 $kg{\cdot}ha^{-1}{\cdot}yr^{-1}$ in 2013 to 5.05 $kg{\cdot}ha^{-1}{\cdot}yr^{-1}$ in 2017 and averaged 2.84 $kg{\cdot}ha^{-1}{\cdot}yr^{-1}$ (Table 2). Over the study period, the NPS loads accounted for 90.8% of the total loads discharged from the

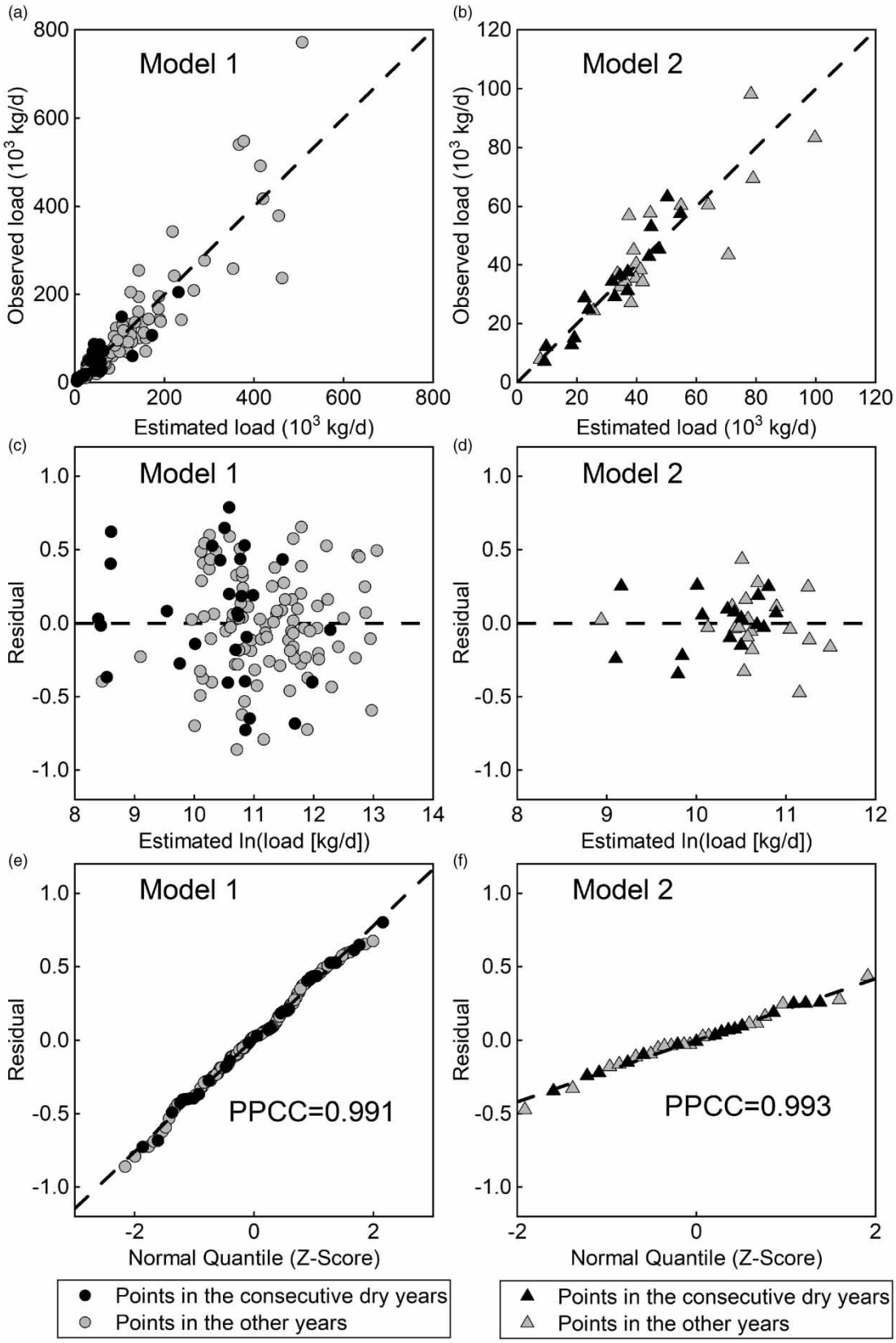

Figure 4 | (a,b) Scatter plots of the observed load versus the estimated load; (c,d) model residuals versus estimates of the log load; and (e,f) normal probability plots for the model residuals.

Table 2 | Summary of the annual precipitation, PS discharge and NO_3-N load, natural runoff, and NPS NO_3-N load

			Natural runoff (mm)					NPS NO_3-N load ($kg \cdot ha^{-1} \cdot yr^{-1}$)				
Year	Annual precipitation (mm)	PS discharge (mm)	Baseflow	Surface runoff	Total natural runoff	*BFI* (%)	PS nitrate load ($kg \cdot ha^{-1} \cdot yr^{-1}$)	Baseflow	Surface runoff	Total nonpoint source	BFNI (%)	BER
2007	989.9	14.6	87.4	219.2	306.6	28.5	0.53	2.14	1.35	3.49	61.2	2.15
2008	947.6	14.6	63.9	152.4	216.2	29.5	0.51	1.50	1.31	2.81	53.3	1.81
2009	887.4	16.0	27.9	85.5	113.4	24.6	0.47	0.70	0.88	1.58	44.2	1.80
2010	974.7	16.5	59.5	190.4	250.0	23.8	0.45	1.63	1.97	3.60	45.2	1.90
2011	***800.5***	***16.6***	***22.0***	***43.4***	***65.3***	***33.6***	***0.32***	***0.71***	***0.40***	***1.12***	***63.8***	***1.90***
2012	***769.6***	***17.0***	***26.0***	***49.2***	***75.1***	***34.6***	***0.32***	***0.96***	***0.25***	***1.21***	***79.2***	***2.29***
2013	***748.1***	***16.8***	***16.3***	***38.1***	***54.4***	***29.9***	***0.32***	***0.67***	***0.36***	***1.03***	***65.3***	***2.18***
2014	939.6	17.5	34.0	99.4	133.3	25.5	0.12	1.26	0.93	2.19	57.4	2.25
2015	934.4	17.7	52.4	146.2	198.6	26.4	0.12	1.70	1.80	3.50	48.5	1.84
2016	1,114.7	18.4	42.4	166.5	209.0	20.3	0.12	1.39	2.32	3.71	37.5	1.85
2017	997.4	21.6	76.1	202.0	278.1	27.3	0.12	1.97	3.08	5.05	39.0	1.42
2018	1,053.0	22.5	57.1	168.1	225.2	25.4	0.12	1.86	2.98	4.84	38.4	1.51
Average over the consecutive dry years	***772.8***	***16.8***	***21.4***	***43.5***	***64.9***	***33.0***	***0.32***	***0.78***	***0.34***	***1.12***	***69.8***	***2.12***
Mean annual average	929.7	17.5	47.1	130.0	177.1	26.6	0.29	1.37	1.47	2.84	48.3	1.82

Note: The bold and italic rows denote the consecutive dry years.

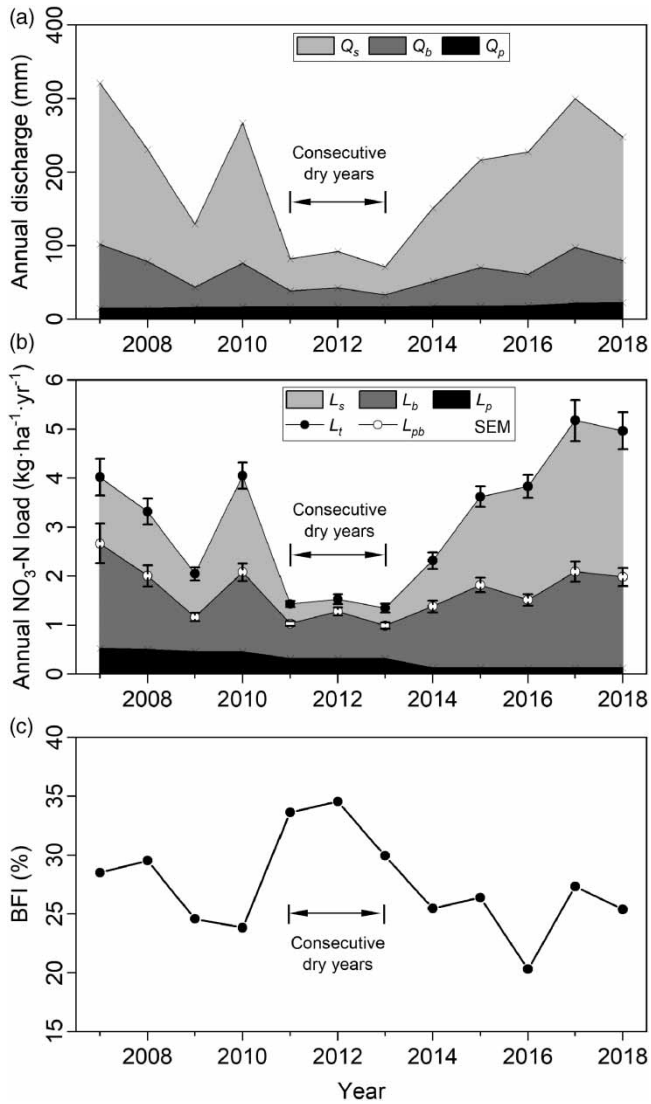

Figure 5 | (a) Annual discharge of PS (Q_p), baseflow (Q_b), and surface runoff (Q_s) in the study period (2007–2018), (b) annual NO_3-N loads contributions of PS (L_p), baseflow (L_b), and surface runoff (L_s), and (c) annual BFI. SEM, standard error of mean.

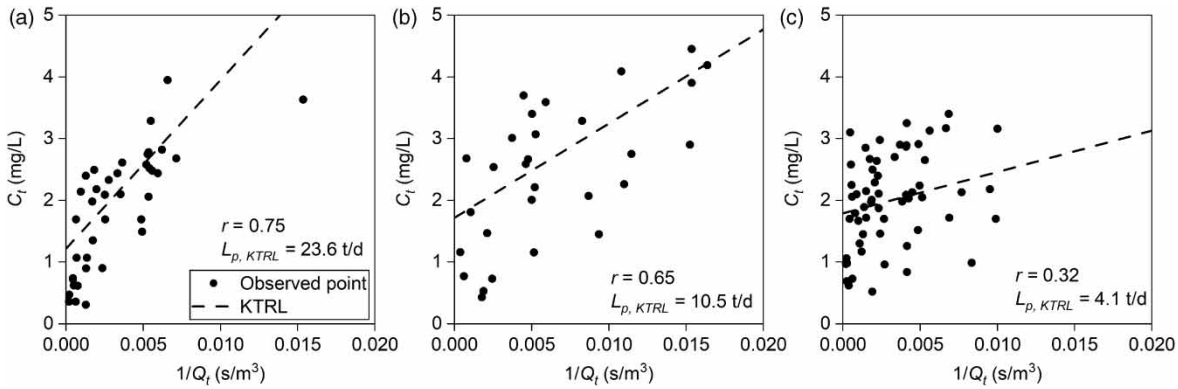

Figure 6 | KTRL regression between the streamflow NO_3-N concentration (C_t) and reciprocal of the total streamflow ($1/Q_t$) in the time periods of (a) 2007–2010, (b) 2011–2013, and (c) 2014–2018. The PS NO_3-N load ($L_{p, KTRL}$) was estimated as the slope of the KTRL, and r is the Pearson correlation coefficient.

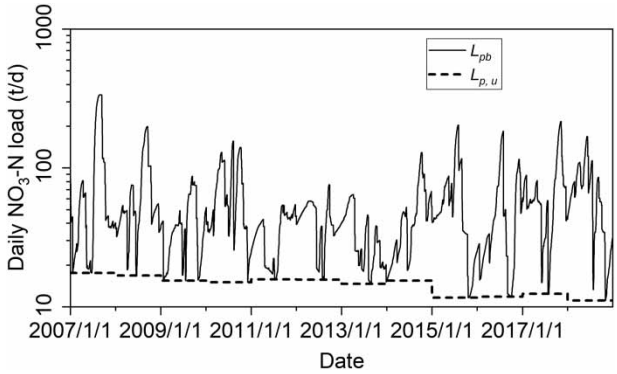

Figure 7 | Estimated daily NO_3-N load attributed to PS and baseflow (L_{pb}) using Model 2 and the upper limit of the PS NO_3-N load ($L_{p,\ u}$).

study area. The temporal variations in the NPS loads were mainly controlled by the rainfall–runoff process, i.e., the NPS load often reached a maximum when the discharges were high (Figure 5(a) and 5(b)). The baseflow NO_3-N load ranged from 0.67 to 2.14 kg·ha^{-1}·yr^{-1} and averaged 1.37 kg·ha^{-1}·yr^{-1}, while the surface runoff NO_3-N load ranged from 0.25 to 3.08 kg·ha^{-1}·yr^{-1} and averaged 1.47 kg·ha^{-1}·yr^{-1} (Table 2). Baseflow and surface runoff contributed 43.8 and 47.0%, respectively, to the total load. The CV was 0.38 and 0.66 for the baseflow and surface runoff loads, respectively. This implies that the baseflow loads were less variable than the surface runoff loads.

The BFNI represents the baseflow contribution to the NPS NO_3-N load. It ranged from 37.5 to 79.2% and averaged 48.3% over the study period (Table 2; Figure 8(a)). The BFNI was the highest in the consecutive dry years with an average of 69.8%, which was higher than the BFNI in the individual dry year (44.2%) and the average over the study period (48.3%). The annual BER in the study area ranged from 1.42 to 2.29 and averaged 1.82 (Table 2; Figure 8(b)).

DISCUSSION

PS and NPS NO_3-N load patterns

Averaged over the 12-year study period, the PS, baseflow, and surface runoff NO_3-N load contributions were 0.29, 1.37, and 1.47 kg·ha^{-1}·yr^{-1}, accounting for 9.2, 43.8, and 47.0% of the total load, respectively. The NO_3-N exported from the upper and middle HRB was mainly attributed to NPSs.

Leather, paper, and chemical fertilizer industries are the main sources of PS NO_3-N load in this area (Li *et al.* 2016), and the denitrification of ammonia nitrogen from domestic sewage is an important indirect source (Ding *et al.* 2018). With the improvement of PS pollution control measures, such as the increase of wastewater treatment plants, the improvement of sewage treatment process, and the upgrading of wastewater discharge standards (He *et al.* 2015), the PS NO_3-N load declined by 77% from 2007 to 2018. This can also be interpreted from Figures 6 and 7. As shown in Figure 6, the slope of the KTRL and the Pearson correlation coefficient (r) between C_t and $1/Q_t$ decreased from 2007 to 2018, and the upper limit of the PS NO_3-N load in Figure 7 also reveals a decreasing trend. Because the NO_3-N concentration is not routinely monitored from the sewage outfalls, the estimated PS NO_3-N load cannot be directly verified. According to the Huai River Water Resources Bulletin (http://www.hrc.gov.cn), both the chemical oxygen demand and ammonia nitrogen (NH_3-N) emissions declined by approximately 70% from 2007 to 2018, which is close to the estimated decline of PS NO_3-N load (77%). This provides indirect evidence for the correctness of the estimated PS NO_3-N loads. In this study, the PS NO_3-N load was estimated based on the data collected at the monitoring station. It represents the exported NO_3-N load attributed to PSs, which was the result of PS NO_3-N transportation and the chemical and biological transformations of PS nitrogen (e.g., nitrification and denitrification) between the source and monitoring station (Albek 2003).

The annual NPS NO_3-N load ranged from 1.03 to 5.05 kg·ha^{-1}·yr^{-1} and averaged 2.84 kg·ha^{-1}·yr^{-1}. The mean annual baseflow NO_3-N load was 1.37 kg·ha^{-1}·yr^{-1} and accounted for 48.3% of the NPS load. This is similar to the result reported for a subbasin in the study area (0.95 kg·ha^{-1}·yr^{-1} for the baseflow NO_3-N load (Chen *et al.* 2017) and 40% for the BFNI (Chen 2013)). N fertilizers have been identified as the main source of NPS NO_3-N pollution in this agricultural watershed (Chen 2013; Ma *et al.* 2019). According to Ju *et al.* (2010), soil residual N and nitrate leaching accounted for about 27 and 30% of the fertilizer N (approximately 600 kg·N·ha^{-1}·yr^{-1}), respectively. The large amount of NO_3-N retained in the soil and

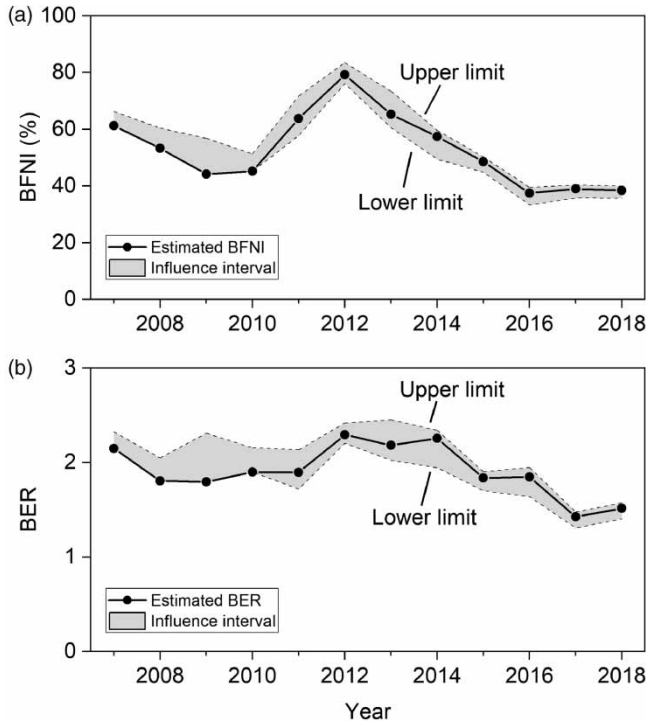

Figure 8 | Annual variations in the estimated (a) BFNI and (b) BER. The influence interval represents the domain of the possible values of the BFNI and BER when considering the errors in PS NO_3-N load estimation.

that leached to groundwater will be transported to surface waters through surface runoff and baseflow. However, the NPS NO_3-N load was much lower in this study area than that in other agricultural watersheds worldwide (Table 3). This may occur due to the high nitrogen uptake rate of crops (Ju & Zhang 2017) and the high denitrification rate in the subsoil zone (Li *et al.* 2020) in the study area. The denitrification in the groundwater (Kolbe *et al.* 2019) and hyporheic zones (Harvey *et al.* 2013) probably also imposes significant impacts and needs to be further investigated in this watershed.

Preferential hydrological pathway of NO_3-N transport

Hydrological processes could be the dominant factors affecting N loss, such as baseflow (Schilling & Zhang 2004), tile drainage (Schilling & Wolter 2001; Deelstra *et al.* 2014), and wet deposition (Povilaitis *et al.* 2014). Various reports have indicated that baseflow is one of the dominant hydrological pathways for NO_3-N migration toward streams (He & Lu 2016). For example, the percentages of total NO_3-N load contributed by baseflow were 66, 59, 52, and 62% for the Raccoon River watershed in the USA (Schilling & Zhang 2004), the Corberia watershed in Spain (Rodríguez-Blanco *et al.* 2013), the Mulgrave River watershed in Australia (Rasiah *et al.* 2013), and the Changle River watershed in China (He *et al.* 2020), respectively. In the upper and middle HRB, the baseflow only accounted for one-fourth of the total natural runoff, while it

Table 3 | The annual NPS NO_3-N load in this and worldwide studies

Region	Agricultural land (%)	Annual runoff (mm)	NPS NO_3-N load ($kg \cdot ha^{-1} \cdot yr^{-1}$)	Citation
Walnut Creek, USA	86	69–865	4–66	Jaynes *et al.* (1999)
Raccoon River, USA	76.2	223	26	Schilling & Zhang (2004)
Upper Sangamon River, USA	87	300	26.4	Guo *et al.* (2002)
Central Germany	66.2	117	18.5–41.2	Rode *et al.* (2009)
Noridc and Baltic countries	35–99	130–1,246	1.7–102.8	Deelstra *et al.* (2014)
Huai River, China	70.1	237.2	2.84	This study

contributed half of the total NPS NO_3-N load. This may result from the higher NO_3-N concentrations in the groundwater (Figure 3). The excessive use of nitrogen fertilizers has caused extremely high NO3-N accumulation in the vadose zone of the study area (Ju & Zhang 2017). Dominated by flatland, this area's groundwater buried depth is generally smaller than 6 m (Ge *et al.* 2006), which makes it easier for the retained NO3-N to leach to groundwater with the infiltration of rainfall. This results in much higher NO_3-N concentrations in groundwater.

The magnitude of BER (Table 2; Figure 8(b)) suggests that baseflow was the preferential hydrological pathway for NO_3-N transport in the upper and middle HRB. The BER in this study area was relatively higher than that in other agricultural watersheds. For example, the BER in the Raccoon River Watershed, USA, ranged from 0.23 to 1.61 and averaged 1.23 (Schilling & Zhang 2004); the BER in the Daejeon region, South Korea, ranged from 0.6 to 1.5 (Kim *et al.* 2010). These results suggest that controlling the baseflow NO_3-N concentration plays a key role in NPS NO_3-N management of the upper and middle HRB.

Influences of the consecutive dry years on the baseflow NO_3-N load

In the consecutive dry years, the reduced runoff resulted in a decrease in the NPS NO_3-N load (Figure 5(a) and 5(b)), while the proportions of the PS and baseflow NO_3-N loads increased. The PS, baseflow, and surface runoff contributions were 22.2, 54.2, and 23.6%, respectively, to the total load. The baseflow was the major contributor to the total load in the consecutive dry years. The BFNI was 25.4% higher in the consecutive dry years than that in the individual dry year (2009), and the BER was 0.32 higher in the consecutive dry years than that in the individual dry year (Table 2). Furthermore, both the BFNI and BER are positively related to the BFI in the study area, as shown in Figure 9. These results suggest that a higher percentage of NO_3-N will be delivered to streams through the baseflow in periods of long-term drought than in short-term drought. Climate change increases the probability of long-term drought (Paxian *et al.* 2019), during which more NO_3-N retained in agricultural soils would leach to groundwater and then transfer to surface waters through baseflow. As a result, the risk of severe NO_3-N pollution in this agricultural area may increase during the dry period. To minimize the NO_3-N pollution in baseflow, appropriate measures should be applied, such as setting the threshold of N fertilizer application rate, limiting N fertilizer application on risk areas, and targeting fertilizer application to periods when crops require N (Andersen *et al.* 2014). In addition, straw return (Li *et al.* 2017), permeable reactive barrier (Zhang *et al.* 2018), and vegetated buffer strips (Janssen *et al.* 2018) are optional practical approaches to minimize the NO_3-N pollution.

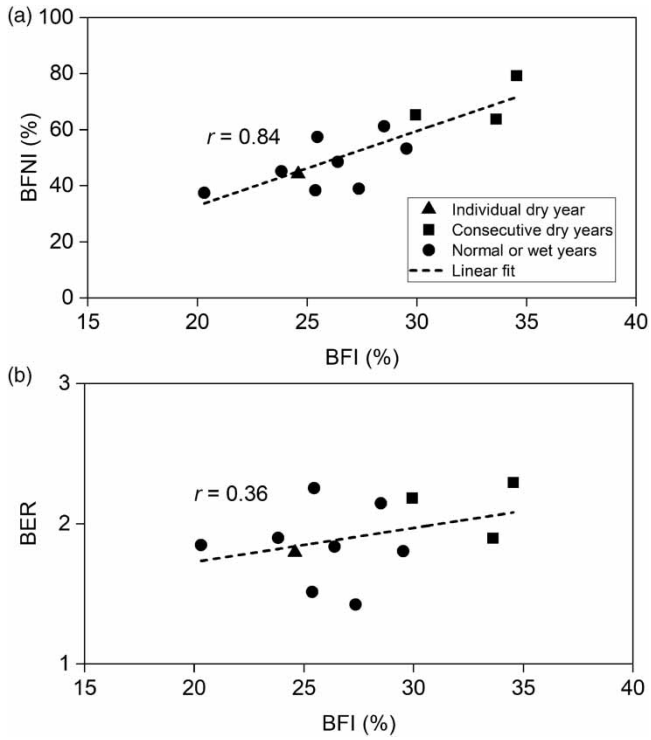

Figure 9 | Relations of the (a) BFNI and (b) BER to the BFI.

Table 4 | Comparison of the natural runoff and NPS NO_3-N load between the time periods before and after the consecutive dry years

		Baseflow		Surface runoff		Total natural runoff	
Time span	Mean annual precipitation (mm)	Discharge (mm)	NO_3-N load ($kg \cdot ha^{-1} \cdot yr^{-1}$)	Discharge (mm)	NO_3-N load ($kg \cdot ha^{-1} \cdot yr^{-1}$)	Discharge (mm)	NO_3-N load ($kg \cdot ha^{-1} \cdot yr^{-1}$)
Period 1 (2007–2010)	949.9	59.7	1.5	161.9	1.38	221.5	2.87
Period 2 (2014–2018)	1,007.8	52.4	1.6	156.4	2.22	208.8	3.86
Change	6.1%	− 12.2%	9.7%	− 3.4%	61.1%	− 5.7%	34.4%

Table 4 provides the mean annual runoff and NPS NO_3-N loads for the periods before and after the consecutive dry years (Periods 1 and 2, respectively). The total natural runoff in Period 2 declined by 5.7% over that in Period 1, while the total NPS NO_3-N load increased by 34.4%. This is mainly the result of the large amounts of NO_3-N storage in the agricultural soils under long-term drought, which were later mobilized in periods of higher rainfall and runoff (Ju & Zhang 2017). Compared to Period 1, the baseflow decreased by 12.2%, while the baseflow NO_3-N load increased by 9.7% in Period 2. The surface runoff decreased by 3.4%, while the surface runoff NO_3-N load increased by 61.1%. This indicates that more NO_3-N was stored on the ground surface than in the groundwater under long-term drought. The surface runoff NO_3-N loads should be controlled, especially after long-term droughts.

Impacts of the errors in PS NO_3-N load estimation

In this study, the PS, baseflow, and surface runoff NO_3-N loads were estimated using LOADEST and KTRL regression. Stenback *et al.* (2011) reported that LOADEST may overestimate the NO_3-N loads for certain rivers, while it performs well at sites with large drainage areas (>20,000 km^2). The drainage area of the upper and middle HRB is much larger than 20,000 km^2. Furthermore, Table 1 and Figure 4 reveal that LOADEST performed well in this area (i.e., NSE >0.75, Bp $< \pm 3$, and RSR < 0.45).

Albek (2003) reported that for nonconservative substances, settling, chemical, and biological transformations between the source and monitoring station could induce uncertainty when estimating the PS NO_3-N load based on the linear regression between the concentration and the reciprocal of the discharge. Because the total NO_3-N load mainly stemmed from NPSs, we mainly analyzed the impacts of the errors in PS NO_3-N load estimation on BFNI and BER. According to Equations (11)–(14), the upper and lower limits of BFNI and BER were calculated, when the PS NO_3-N load ranged from 0 to its upper limit (Figure 7). A small influence interval (the difference between the upper and lower limits) indicates a nonsignificant impact of the PS NO_3-N load errors on the BFNI and BER. It is evident from Figure 8 that the influence intervals for the BFNI (4.3–14.0%) and BER (0.17–0.52) are relatively small, and the characteristics of the interannual variations in the BFNI and BER have few changes. For example, the mean BFNI was higher in the consecutive dry years (64.9–76.3%) than that in the individual dry year (44.2–56.9%), while the BER, ranging from 1.31 to 2.45, was higher than 1 in all years. Therefore, it is reasonable to conclude that the errors in PS NO_3-N load estimation imposed nonsignificant impacts on the BFNI and BER in this work.

Although a physical basis is lacking, the combined methods applied in this study could provide a rough estimation of the NO_3-N loads consisting of PS, baseflow, and surface runoff contributions for regions where the PS load cannot be neglected and wastewater monitoring is not performed. Compared to physically based hydrological process models (He & Lu 2016), the above-combined methods require less data (mainly concentration and discharge data measured at monitoring stations). It is a good choice to use the combined methods to separate the PS, baseflow, and surface runoff NO_3-N loads from the total load when few PS monitoring data are available.

CONCLUSIONS

Over a 12-year study period, the PS, baseflow, and surface runoff NO_3-N loads were quantified in the upper and middle HRB. The PS, baseflow, and surface runoff contributions were 9.2, 43.8, and 47.0%, respectively, to the mean annual total load (3.13 $kg \cdot ha^{-1} \cdot yr^{-1}$). The baseflow accounted for approximately one-fourth of the total natural runoff and contributed half of the total NPS NO_3-N load, and the mean annual BER was 1.82. The BFNI and BER were higher in the consecutive

dry years (69.8% and 2.12, respectively) than those in the individual dry years (44.2% and 1.80, respectively). We have demonstrated that NPSs are the major contributors to the total NO_3-N load and that baseflow is the primary hydrological pathway for NO_3-N transport in this area. Compared to short-term drought, a higher percentage of NO_3-N will be delivered to streams through baseflow under long-term drought. This study highlights the alarming evidence that continuous drought caused by climate change may lead to a higher rate of nitrogen loss in agricultural watersheds. Therefore, controlling the baseflow NO_3-N load (e.g., fertilizer application rate control, vegetated buffer strips, straw return, and permeable reactive barrier) plays a key role in NPS NO_3-N management of the upper and middle HRB, especially in dry periods that span consecutive years.

ACKNOWLEDGEMENTS

This work was supported by the Major Projects of Science and Technology for Water Pollution Control and Management (Grant/Award Nos 2012ZX07204-003 and 2017ZX07602-003). The authors thank Xushui Cheng, Kailai Qian, and Tiansong Qi for their assistance with data collection. We also thank Chengpeng Lu for his valuable suggestions.

DATA AVAILABILITY STATEMENT

All relevant data are available from an online repository or repositories (https://doi.org/10.6084/m9.figshare.14167403.v2).

REFERENCES

Albek, E. 2003 Estimation of point and diffuse contaminant loads to streams by non-parametric regression analysis of monitoring data. *Water, Air, and Soil Pollution* **147** (1), 229–243. http://doi.org/10.1023/A:1024592815576.

Almasri, M. N. & Kaluarachchi, J. J. 2004 Assessment and management of long-term nitrate pollution of ground water in agriculture-dominated watersheds. *Journal of Hydrology* **295** (1–4), 225–245. http://doi.org/10.1016/j.jhydrol.2004.03.013.

An, G. & Hao, Z. 2017 Variation of precipitation and streamflow in the Upper and Middle Huaihe River Basin, China, from 1959–2009. *Journal of Coastal Research* **80** (sp1), 69–79. http://doi.org/10.2112/SI80-010.1.

Andersen, H. E., Blicher-Mathiesen, G., Bechmann, M., Povilaitis, A., Iital, A., Lagzdins, A. & Kyllmar, K. 2014 Mitigating diffuse nitrogen losses in the Nordic-Baltic countries. *Agriculture, Ecosystems & Environment* **195**, 53–60. http://doi.org/10.1016/j.agee.2014.05.009.

Barlow, P. M., Cunningham, W. L., Zhai, T. & Gray, M. 2015 *U.S. Geological Survey Groundwater Toolbox, a Graphical and Mapping Interface for Analysis of Hydrologic Data (Version 1.0): User Guide for Estimation of Base Flow, Runoff, and Groundwater Recharge from Streamflow Data*. U.S. Geological Survey Techniques and Methods, book 3, chap. B10, 27 p. http://dx.doi.org/10.3133/tm3B10.

Chen, L. 2013 *Modeling of the Water Flow and Nitrate Transport in the Shallow Aquifer of the Shaying River Basin and Its Contribution to River Pollution*. M.S. Thesis, School of Earth Science and Engineering, Nanjing University, Nanjing, China (in Chinese).

Chen, Z., Ruan, X. & Shan, N. 2017 Modeling of nitrate flux between groundwater and surface water based on a coupled model in Shaying River Basin. *Journal of Nanjing University (Natural Science)* **53** (5), 860–870 (in Chinese).

Cohn, T. A., Delong, L. L., Gilroy, E. J., Hirsch, R. M. & Wells, D. K. 1989 Estimating constituent loads. *Water Resources Research* **25** (5), 937–942. http://doi.org/10.1029/WR025i005p00937.

Coskun, D., Britto, D. T., Shi, W. M. & Kronzucker, H. J. 2017 Nitrogen transformations in modern agriculture and the role of biological nitrification inhibition. *Nature Plants* **3**, 17074. http://doi.org/10.1038/nplants.2017.74.

Czekaj, J., Jakobczyk-Karpierz, S., Rubin, H., Sitek, S. & Witkowski, A. J. 2016 Identification of nitrate sources in groundwater and potential impact on drinking water reservoir (Goczalkowice reservoir, Poland). *Physics and Chemistry of the Earth* **94**, 35–46. http://doi.org/10.1016/j.pce.2015.11.005.

Deelstra, J., Iital, A., Povilaitis, A., Kyllmar, K., Greipsland, I., Blicher-Mathiesen, G., Jansons, V., Koskiaho, J. & Lagzdins, A. 2014 Hydrological pathways and nitrogen runoff in agricultural dominated catchments in Nordic and Baltic countries. *Agriculture, Ecosystems & Environment* **195**, 211–219. http://doi.org/ 10.1016/j.agee.2014.06.007.

de Graaf, I. E. M., Gleeson, T., van Beek, L. P. H., Sutanudjaja, E. H. & Bierkens, M. F. P. 2019 Environmental flow limits to global groundwater pumping. *Nature* **574** (7776), 90–94. http://doi.org/10.1038/s41586-019-1594-4.

Ding, S. Z., Bao, P., Wang, B., Zhang, Q. & Peng, Y. Z. 2018 Long-term stable simultaneous partial nitrification, anammox and denitrification (SNAD) process treating real domestic sewage using suspended activated sludge. *Chemical Engineering Journal* **339**, 180–188. http://doi.org/10.1016/j.cej.2018.01.128.

Eckhardt, K. 2005 How to construct recursive digital filters for baseflow separation. *Hydrological Processes* **19** (2), 507–515. http://doi.org/10.1002/hyp.5675.

Eckhardt, K. 2008 A comparison of baseflow indices, which were calculated with seven different baseflow separation methods. *Journal of Hydrology* **352** (1–2), 168–173. http://doi.org/10.1016/j.jhydrol.2008.01.005.

Ge, W. Y., Ye, N. J., Gong, J. S., Yu, J. J., Zuo, Z. J., Yang, Z. D. & Huang, J. J. 2006 The quaternary aquifer division and character analysis of plain in Huaihe River basin. *Resources Survey & Environment* **27** (4), 268–276 (in Chinese).

Guo, Y. P., Markus, M. & Demissie, M. 2002 Uncertainty of nitrate-N load computations for agricultural watersheds. *Water Resources Research* **38** (10), 13. http://doi.org/10.1029/2001wr001149.

Harvey, J. W., Bohlke, J. K., Voytek, M. A., Scott, D. & Tobias, C. R. 2013 Hyporheic zone denitrification: controls on effective reaction depth and contribution to whole-stream mass balance. *Water Resources Research* **49** (10), 6298–6316. http://doi.org/10.1002/wrcr.20492.

He, S. & Lu, J. 2016 Contribution of baseflow nitrate export to non-point source pollution. *Science China Earth Sciences* **59** (10), 1912–1929. http://doi.org/10.1007/s11430-016-5329-1.

He, T., Lu, Y., Cui, Y., Luo, Y., Wang, M., Meng, W., Zhang, K. J. & Zhao, F. 2015 Detecting gradual and abrupt changes in water quality time series in response to regional payment programs for watershed services in an agricultural area. *Journal of Hydrology* **525**, 457–471. http://doi.org/10.1016/j.jhydrol.2015.04.005.

He, S., Hao, Y., Wu, J. & Lu, J. 2020 Estimation of baseflow nitrate loads by a recursive tracing source algorithm in a rainy agricultural watershed. *Hydrological Processes* **34** (2), 441–454. http://doi.org/10.1002/hyp.13597.

Helsel, D. R. & Hirsch, R. M. 1992 *Statistical Methods in Water Resources*. Elsevier, The Netherlands.

Janssen, M., Frings, J. & Lennartz, B. 2018 Effect of grass buffer strips on nitrate export from a tile-drained field site. *Agricultural Water Management* **208**, 318–325. http://doi.org/10.1016/j.agwat.2018.06.026.

Jaynes, D. B., Hatfield, J. L. & Meek, D. W. 1999 Water quality in Walnut Creek Watershed: Herbicides and nitrate in surface waters. *Journal of Environmental Quality* **28** (1), 45. https://doi.org/ 28.10.2134/jeq1999.00472425002800010005x.

Ju, X. T. & Zhang, C. 2017 Nitrogen cycling and environmental impacts in upland agricultural soils in North China: a review. *Journal of Integrative Agriculture* **16** (12), 2848–2862. http://doi.org/10.1016/S2095-3119(17)61743-X.

Ju, X. T., Liu, X. J. & Zhang, L. J. 2010 Nitrogen cycling and ecoenvironment effect of winter wheat-summer maize rotation in North China Plain (in Chinese). In: *Fundamental Research on Fate and Efficient Use of Nitrogen Fertilizer in Main Agroecosystems* (Z. L. Zhu, ed.), 1st edn. Science Press, China, pp. 55–106.

Kim, G., Lee, H., Lim, Y., Jung, M. & Kong, D. 2010 Baseflow contribution to nitrates in an urban stream in Daejeon, Korea. *Water Science and Technology* **61**, 3216–3220. http://doi.org/10.2166/wst.2010.245.

Kolbe, T., de Dreuzy, J. R., Abbott, B. W., Aquilina, L., Babey, T., Green, C. T., Fleckenstein, J. H., Labasque, T., Laverman, A. M., Marcais, J., Peiffer, S., Thomas, Z. & Pinay, G. 2019 Stratification of reactivity determines nitrate removal in groundwater. *Proceedings of the National Academy of Sciences* **116** (7), 2494–2499. http://doi.org/10.1073/pnas.1816892116.

Li, N., Yang, H., Wang, L. C., Huang, X. J., Zeng, C. F., Wu, H., Ma, X. X., Song, X. T. & Wei, Y. N. 2016 Optimization of industry structure based on water environmental carrying capacity under uncertainty of the Huai River Basin within Shandong Province, China. *Journal of Cleaner Production* **112**, 4594–4604. http://doi.org/10.1016/j.jclepro.2015.08.074.

Li, R. F., Ruan, X. H., Bai, Y., Ma, T. H. & Liu, C. Q. 2017 Effect of wheat-maize straw return on the fate of nitrate in groundwater in the Huaihe River Basin, China. *Science of the Total Environment* **592**, 78–85. http://doi.org/10.1016/j.scitotenv.2017.03.029.

Li, R. F., Ruan, X. H., Ma, T. H., Bai, Y. & Liu, C. Q. 2020 In-situ nitrogen fate in the vadose zone of different soil types and its implications for groundwater quality in the Huaihe River Basin, China. *Acta Geochimica* **39** (3), 281–290. http://doi.org/10.1007/s11631-020-00412-8.

Ma, P., Liu, S. X., Yu, Q. B., Li, X. Y. & Han, X. Q. 2019 Sources and transformations of anthropogenic nitrogen in the highly disturbed Huai River Basin, Eastern China. *Environmental Science and Pollution Research* **26** (11), 11153–11169. http://doi.org/10.1007/s11356-019-04470-1.

Moriasi, D. N., Arnold, J. G., Van Liew, M. W., Bingner, R. L., Harmel, R. D. & Veith, T. L. 2007 Model evaluation guidelines for systematic quantification of accuracy in watershed simulations. *Transactions of the ASABE* **50** (3), 885–900. http://doi.org/10.13031/2013.23153.

Paladino, O., Massabo, M. & Gandoglia, E. 2020 Assessment of nitrate hazards in Umbria Region (Italy) using field datasets: good agriculture practices and farms sustainability. *Sustainability* **12**, 22. http://doi.org/10.3390/su12229497.

Pan, Z. R. 2014 *Study on the Influence of Baseflow on the Environmental Flow in Huai River Basin, China*. PhD Thesis, School of Earth Science and Engineering, Nanjing University, Nanjing, China (in Chinese).

Paxian, A., Ziese, M., Kreienkamp, F., Pankatz, K., Brand, S., Pasternack, A., Pohlmann, H., Modali, K. & Fruh, B. 2019 User-oriented global predictions of the GPCC drought index for the next decade. *Meteorologische Zeitschrift* **28** (1), 3–21. http://doi.org/10.1127/metz/2018/0912.

Povilaitis, A., Šileika, A., Deelstra, J., Gaigalis, K. & Baigys, G. 2014 Nitrogen losses from small agricultural catchments in Lithuania. *Agriculture, Ecosystems & Environment* **198**, 54–64. http://doi.org/10.1016/j.agee.2014.02.002.

Rasiah, V., Armour, J. D. & Nelson, P. N. 2013 Nitrate in shallow fluctuating groundwater under sugarcane: quantifying the lateral export quantities to surface waters. *Agriculture, Ecosystems & Environment* **180**, 103–110. http://doi.org/10.1016/j.agee.2012.07.002.

Richards, G., Gilmore, T. E., Mittelstet, A. R., Messer, T. L. & Snow, D. D. 2021 Baseflow nitrate dynamics within nested watersheds of an agricultural stream in Nebraska, USA. *Agriculture Ecosystems & Environment* **308**. http://doi.org/10.1016/j.agee.2020.107223.

Rode, M., Thiel, E., Franko, U., Wenk, G. & Hesser, F. 2009 Impact of selected agricultural management options on the reduction of nitrogen loads in three representative meso scale catchments in Central Germany. *Science of the Total Environment* **407** (11), 3459–3472. http://doi.org/10.1016/j.scitotenv.2009.01.053.

Rodríguez-Blanco, M. L., Taboada-Castro, M. M. & Taboada-Castro, M. T. 2013 Contrasting dynamics of nitrate and kjeldahl nitrogen in a stream draining a rural catchment in Galicia (NW Spain). *Communications in Soil Science and Plant Analysis* **44** (1–4), 415–421. http://doi.org/10.1080/00103624.2013.742333.

Runkel, R. L., Crawford, C. G. & Cohn, T. A. 2004 *Load Estimator (LOADEST) – A FORTRAN Program for Estimating Constituent Loads in Streams and Rivers*. U.S. Geological Survey Techniques and Methods, Book 4, 69 p. (Chapter A5), U.S. Geological Survey, Reston, VA.

Schilling, K. E. & Wolter, C. 2001 Contribution of base flow to nonpoint source pollution loads in agricultural watershed. *Ground Water* **39**, 49–58.

Schilling, K. E. & Zhang, Y. K. 2004 Baseflow contribution to nitrate-nitrogen export from a large, agricultural watershed, USA. *Journal of Hydrology* **295** (1–4), 305–316. http://doi.org/10.1016/j.jhydrol.2004.03.010.

Stenback, G. A., Crumpton, W. G., Schilling, K. E. & Helmers, M. J. 2011 Rating curve estimation of nutrient loads in Iowa rivers. *Journal of Hydrology* **396** (1–2), 158–169. http://doi.org/10.1016/j.jhydrol.2010.11.006.

Wu, H., Dong, Y., Gao, L., Song, X., Liu, F., Peng, X. & Zhang, G. 2021 Identifying nitrate sources in surface water, regolith and groundwater in a subtropical red soil Critical Zone by using dual nitrate isotopes. *Catena* **198**. http://doi.org/10.1016/j.catena.2020.104994.

Zhang, W., Ruan, X. H., Bai, Y. & Yin, L. 2018 The characteristics and performance of sustainable-releasing compound carbon source material applied on groundwater nitrate in-situ remediation. *Chemosphere* **205**, 635–642. http://doi.org/10.1016/j.chemosphere.2018.04.133.

First received 27 September 2020; accepted in revised form 25 May 2021. Available online 18 June 2021